Nanoparticle Diffusion in Crowded Polymer Nanocomposite Melts

Kaitlin Wang[1] and Karen I. Winey[1,2, *]

[1] Department of Materials Science and Engineering, University of Pennsylvania, Philadelphia, PA 19104, United States of America

[2] Department of Chemical and Biomolecular Engineering, University of Pennsylvania, Philadelphia, PA 19104, United States of America

***Corresponding author: Karen I. Winey, winey@seas.upenn.edu,**

Address: Laboratory for Research on the Structure of Matter, 3231 Walnut St, Philadelphia, PA 19104

For Table of Contents Use only

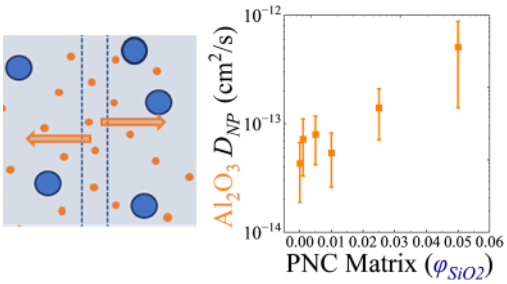

Abstract

This study examines nanoparticle diffusion in crowded polymer nanocomposites by diffusing small Al_2O_3 nanoparticles (NPs) in SiO_2-loaded P2VP matrices. Time-of-flight secondary ion mass spectroscopy (ToF-SIMS) measures Al_2O_3 NP diffusion coefficients within a homogeneous PNC background of larger, immobile SiO_2 NPs. By developing a geometric model for average interparticle distance in a system with two NP sizes, we quantify nanocomposite confinement relative to the Al_2O_3 NP size with a bound layer. At low SiO_2 concentrations, Al_2O_3 NP diffusion aligns with neat polymer results. In more crowded nanocomposites with higher SiO_2 concentrations where the interparticle distance approaches the size of the mobile Al_2O_3 NP, the 6.5-nm Al_2O_3 NPs diffuse faster than predicted by both core-shell and vehicular diffusion models. Relative to our previous studies of NPs diffusing into polymer, these findings demonstrate that the local environment in crowded systems significantly complicates NP diffusion behavior and the bound layer lifetimes.

Keywords: polymer nanocomposites, nanoparticle diffusion, confinement, ToF-SIMS

Incorporating nanoparticles into polymer nanocomposites (PNCs) enhances material characteristics and allows tunability.[1–5] Understanding diffusion in crowded nanocomposites is crucial for predicting material behavior, impacting fields like drug delivery and advanced materials.[6–8] Crowded PNCs simulate densely packed environments, allowing control over matrix and nanoparticle (NP) parameters.[7,9] Polymers and NPs in confined environments experience unique interactions due to spatial restrictions[10] and increased surface area,[11–13] altering their behaviors compared to dilute environments.

Previous work highlights the impact of nanoparticle attributes on polymer dynamics. Interaction strength, NP size, and NP distribution can alter the glass transition temperature[12,14] and mechanical properties. Particle loading's effect on polymer diffusion has been studied in both athermal and attractive PNC systems.[15–17] With attractive interactions, including the P2VP/SiO_2/Al_2O_3 PNC system of this work, the polymer diffusion coefficient drops by fivefold with increasing NP concentration and remains depressed even at interparticle distances (ID) >> $2R_g$.[18]

Nanoparticle diffusion in crowded environments differs from classical Brownian motion as crowding effects dominate.[17,19,20] Xue et al. reported hopping diffusion and polymer network interactions influencing NP diffusion when NP size is comparable to or smaller than the polymer matrix mesh size.[21] Many studies on NP diffusion in crowded media focus on polymer solutions[22] or gels[23] that are compatible with low particle concentrations.

Here, we measure NP diffusion coefficients of small Al_2O_3 nanoparticles into polymer nanocomposites of large well-dispersed[24–29] SiO_2 nanoparticles with loading from dilute to crowded (φ_{SiO2} = 0.001 – 0.05). Using time-of-flight secondary ion mass spectrometry (ToF-

SIMS), our previously demonstrated method,[30] we distinguish between diffusing Al_2O_3 and background SiO_2 nanoparticles in the PNC with two NP sizes. **Figure 1** illustrates idealized Al^+ concentration profiles before and after annealing.

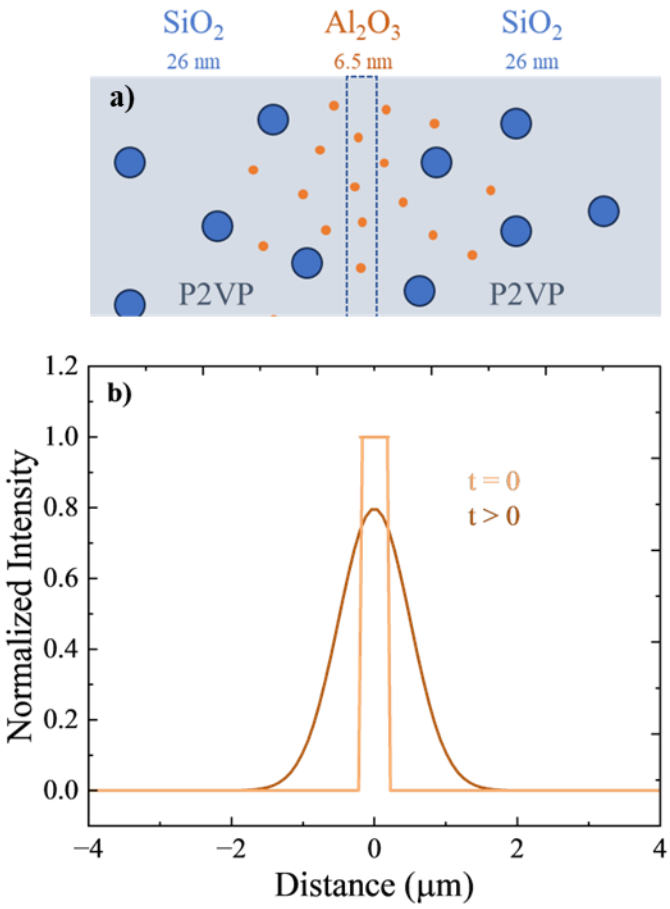

Figure 1: Schematic and concentration profiles of small Al_2O_3 NPs diffusing into SiO_2-P2VP layers. (**a**) Cross-sectional view of the trilayer sample with a central Al_2O_3 NP layer ($\varphi_{Al2O3} = 0.01$, orange) diffusing into the surrounding SiO_2-loaded P2VP matrix (blue). **b)** Representational concentration profiles before ($t = 0$) and after annealing ($t > 0$) showing Al_2O_3 NP diffusion into the SiO_2-P2VP nanocomposite.

The initial concentration of Al_2O_3 nanoparticles in the mid-layer is $\varphi_{Al2O3} = 0.01$. Following precedent set by previous polymer[31–38] and NP[25,26,39,40] diffusion studies in bilayer and trilayer geometries, we use a trilayer sample geometry to measure diffusion coefficients. Each trilayer

sample was annealed for 1, 3, and 6 hours and the normalized Al^+ concentration profiles were fit to Fick's second law solution for a finite source diffusing into a semi-infinite medium,

$$\varphi(y) = \frac{1}{2}\left[\mathrm{erf}\left(\frac{h-y}{\sqrt{4D_{NP}t}}\right) + \mathrm{erf}\left(\frac{h+y}{\sqrt{4D_{NP}t}}\right)\right] \quad (1)$$

where $\varphi(y)$ is the concentration as a function of position y, h is the film's initial thickness (~ 0.2 μm), D_{NP} is the NP diffusion coefficient, and t is the annealing time in seconds. **Figure 2** and **Figure S2** present time series showing the progression of Al_2O_3 NPs moving into a SiO_2-P2VP nanocomposite (φ_{SiO2} = 0.025) when annealed at 180°C (~ T_g + 50°C) along with best fits to Eqn. 1 to give experimental D_{NP} values, **Table S1**.

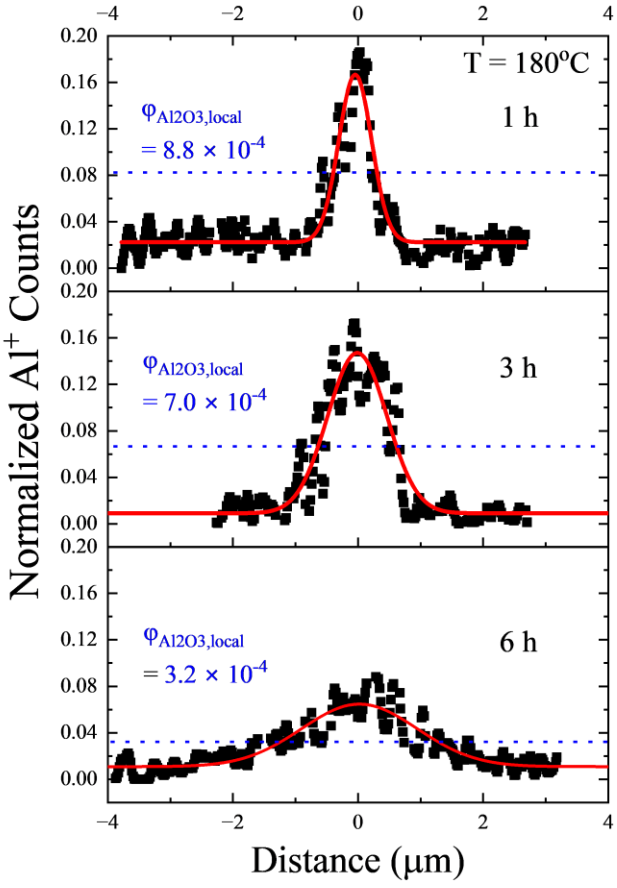

Figure 2: Concentration profiles of Al^+ ions indicating the spatial distribution of Al_2O_3 NPs within a SiO_2-P2VP nanocomposite (φ_{SiO2} = 0.025). The samples, with an initial φ_{Al2O3} = 0.01

concentration in the mid-layer, were annealed at 180 °C for 1, 3, and 6 hours. The local Al_2O_3 concentrations, $\varphi_{Al2O3,local}$, are the concentration at the full-width at half maxima (FWHM) of the normalized concentration profiles (blue). Red lines are best fits of Eqn. 1.

The Schweizer group proposed two simultaneous mechanisms of NP diffusion in nanocomposites with dilute monodisperse spherical NPs: core-shell and vehicular modes of NP diffusion.[41,42]

$$D_{NP,theory} = D_{core\text{-}shell} + D_{vehicle} \quad (2)$$

The core-shell mode is a modified Stokes-Einstein model accounting for the increased NP radius due to the bound layer (R_{eff}) and the increased viscosity in nanocomposites (η_{PNC}),

$$D_{core-shell} = \frac{k_B T}{6\pi\eta_{PNC} R_{eff}} \quad (3)$$

$$\eta_{PNC} = \eta_{poly}(1 + 2.5\varphi_{eff} + 6.2{\varphi_{eff}}^2) \quad (4)$$

where η_{poly} is the viscosity of the neat polymer and φ_{eff} accounts for R_{eff}. Core-shell diffusion has been demonstrated with quantum dots in poly(propylene glycol) (PPG), SiO_2 NPs in PPG, and SiO_2 NPs in P2VP.[41,43–45]

Vehicular diffusion is influenced by monomeric desorption times (τ_{des}) from NP surfaces and is partitioned into three regimes based on the desorption time relative to polymer dynamic time scales (entanglement onset time, τ_e, Rouse time, τ_{Rouse}, and reptation time, τ_{Rep}). For the 158 kDa P2VP at 180 °C, τ_e = 0.90 s and τ_{Rouse} = 70 s.[45,46] Regime I corresponds to the fastest desorption times ($\tau_{des} < \tau_e$) and is not relevant to our system due to hydrogen bonding between the Al_2O_3 NPs and P2VP. Regime III describes the slowest desorption times $\tau_{Rouse} < \tau_{des} < \tau_{rep}$ and is not relevant in this system. Notably, in our recent work,[45] we established that 6.5-nm Al_2O_3 NPs diffusing into neat P2VP transition from predominantly core-shell diffusion to vehicular

Regime II diffusion as polymer molecular weight increases from 14 - 1220 kDa. We found $\tau_{des}\sim$ 50 s at 180 °C, which is intermediate between τ_e and τ_{Rouse}. This intermediate desorption time corresponds to Regime II and $D_{vehicle-II}$ is inversely proportional to ${\tau_{des}}^{3/4}$,

$$D_{vehicle-II} = Ad_T(b^2D_0)^{\frac{1}{4}} \times \left(\frac{1}{\tau_{\mathrm{des}}}\right)^{\frac{3}{4}} \quad (5)$$

where A is a numerical prefactor, d_T is the tube diameter, b is the Kuhn monomer length, and D_0 is the segmental diffusion constant. For the following calculations, A = 1, d_T = 23.5 nm, b = 1.8 nm, and $D_0 = 1.0 \times 10^{-9}$ cm^2/s.[45,46] The Al_2O_3 NP diffusion into neat 158 kDa P2VP is well described by $D_{NP,theory}$ (Eqn. 2), that accounts for the increased viscosity of the NP loading and bound polymer layer thickness (Eqn. 3) and vehicular motion from polymer desorption (Eqn. 5).

Figure 3 presents D_{NP} for the small NPs as a function of the concentration of the large NPs, φ_{SiO2}. In neat 158 kDa P2VP ($\varphi_{SiO2} = 0$), we previously[45] demonstrated that these Al_2O_3 NPs have a diffusion coefficient of 4.3 ± 2.4 × 10^{-14} cm²/s (Figure 3). When the Al_2O_3 NPs diffuse into nanocomposites, as studied here, we begin by comparing the measured D_{NP} with $D_{NP,theory}$ (Eqn. 2). At dilute PNC loadings, the D_{NP} agrees with $D_{core\text{-}shell}$ + $D_{vehicleII}$ with $\tau_{des}\sim$ 50 s (dotted line), consistent with our previous neat P2VP results. At higher PNC loading, D_{NP} deviates by an order of magnitude from this prediction, which suggests a shorter τ_{des} in crowded systems. Specifically, τ_{des} decreases from 20 s to 1.4 s as φ_{SiO2} increases from 0.001 to 0.050, **Table S2.**

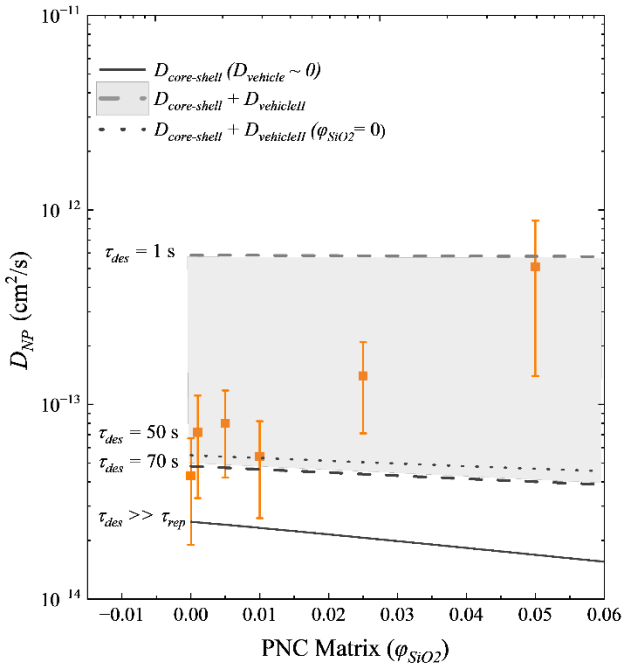

Figure 3: D_{NP} (orange) as a function of matrix SiO_2 NP loading. Samples were annealed for 1-6 hours. Benchmark diffusion measurements of Al_2O_3 NPs into a neat P2VP matrix (φ_{SiO2} = 0) were annealed 12 – 72 hours. Line indicate $D_{core\text{-}shell}$ (solid), $D_{core\text{-}shell}$ + $D_{vehicleII}$ [dashed, upper (τ_{des} ~ 1 s) and lower (τ_{des} ~ 70 s)], and $D_{core\text{-}shell}$ + $D_{vehicleII}$ (dotted, τ_{des} ~ 50).

Here, Al_2O_3 NPs diffuse into SiO_2-P2VP nanocomposites, creating Al_2O_3-SiO_2-P2VP nanocomposites. To account for the increasing Al_2O_3 NP concentration in the surrounding SiO_2-P2VP nanocomposite, we define the local time-dependent concentration for Al_2O_3 NPs, $\varphi_{Al2O3,local}$. The normalized intensity at the FWHM of the Al^+ concentration profiles, Figure 2, is scaled by the initial concentration of the nanoparticles in the film to give $\varphi_{Al2O3,local}$, Table S3.

The NP surface-to-surface interparticle distance, *ID*, quanitifies crowding as a function of particle size and loading, and is crucial for understanding polymer diffusion in nanocomposites.[8,17,47] In addition to using initial Al_2O_3 NP concentration of φ_{Al2O3} = 0.01, we also explored higher initial concentrations of φ_{Al2O3} = 0.05 and found overlapping concentration profiles

upon annealing 1-7 days (see Table S4 and Figure S3) indicating the absence of NP tracer diffusion. Using the equations developed below, these experiments have interparticle distances smaller than the effective size of the Al_2O_3 NPs. This example of non-Fickian diffusion in a crowded system demonstrates the importance of the bound polymer layers and the bimodal interparticle distance, ID_{bi}, relative to the size of the diffusing species.

In a monodisperse system of spherical nanoparticles, *ID* is [48]

$$ID = 2r_{NP}[\left(\frac{\varphi_{max}}{\varphi_{NP}}\right)^{\frac{1}{3}} - 1] \quad (6)$$

where φ_{max} is the nanoparticle volume fraction at maximum packing, φ_{NP} is the volume fraction of NPs, and r_{NP} is the radius of the nanoparticle. For this study, we extend Eqn. 6 to consider two nanoparticle sizes. Using geometric arguments involving cells that include the volume of an average particle and the excess volume per particle, we express the number-averaged *ID* in a bimodal-sized NP system as

$$ID_{bi} = 2(r_{cell} - \bar{r}_{NP}) = 2([r_L^3 * \frac{n_L}{n_T} + r_s^3 \frac{n_s}{n_{Total}} + \frac{3}{4\pi}\psi]^{\frac{1}{3}} - \bar{r}_{NP})) \quad (7)$$

$$\psi = \frac{(\varphi_{max-bi} - \varphi_L - \varphi_S)}{\frac{\varphi_L}{\frac{4}{3}\pi {r_L}^3} + \frac{\varphi_S}{\frac{4}{3}\pi {r_S}^3}} \quad (8)$$

where r_{cell} is derived from the volume of a cell ~ ${V_{cell}}^{1/3}$; $\bar{r}_{NP}$ is the number average radius of the two particles; r_L, n_L and φ_L are the radius, number and volume fraction of the large particles; r_S, n_S and φ_S are the radius, number and volume fraction of the small particles; n_{Total} is the total number of particles; ψ is the excess volume per particle; and φ_{max-bi} is the maximum nanoparticle volume fraction in a bimodal system. The full derivation is in **Supporting Information**. In our experiments, the large nanoparticles are SiO_2 with r_L = 26 nm, the small nanoparticles are Al_2O_3 with r_S = 6.5 nm.

Our expression for ID_{bi} uses fixed Al_2O_3 and SiO_2 concentrations. While the concentration of SiO_2 NPs is uniform and independent of annealing time, the concentration of Al_2O_3 NPs evolves with annealing time (see Figure 2). We use the local time-dependent loading of Al_2O_3 NPs, $\varphi_{Al2O3,local}$, as the concentration of small nanoparticles, $\varphi_S = \varphi_{Al2O3,local}$. Thus, at fixed SiO_2 NP concentrations, as diffusion continues and $\varphi_{Al2O3,local}$ decreases, the average ID_{bi} increases, **Figure 4** (dashed curves).

Next, we account for the polymer bound layer, which has been previously established to be ~R_g in polymer melt systems,[40,49–51] associated with strong polymer-NP interactions. The effective NP radii, $r_{L,eff}$ and $r_{S,eff}$, are the nanoparticle radii plus the radius of gyration of the 158 kDa P2VP (R_g = 10.9 nm). The presence of bound layer also increases the NP concentrations to effective NP concentration, $\varphi_{L,eff}$, and $\varphi_{S,eff}$, and given by[43]

$$\varphi_{L,eff} = \varphi_{SiO2}\left(\frac{r_{L,eff}}{r_L}\right)^3 \quad (9)$$

$$\varphi_{S,eff} = \varphi_{Al2O3,local}\left(\frac{r_{S,eff}}{r_S}\right)^3 \quad (10)$$

Relative to nanocomposites with bare nanoparticles, ID_{bi} is smaller when the bound layer is included, **Figure 4** (solid lines).

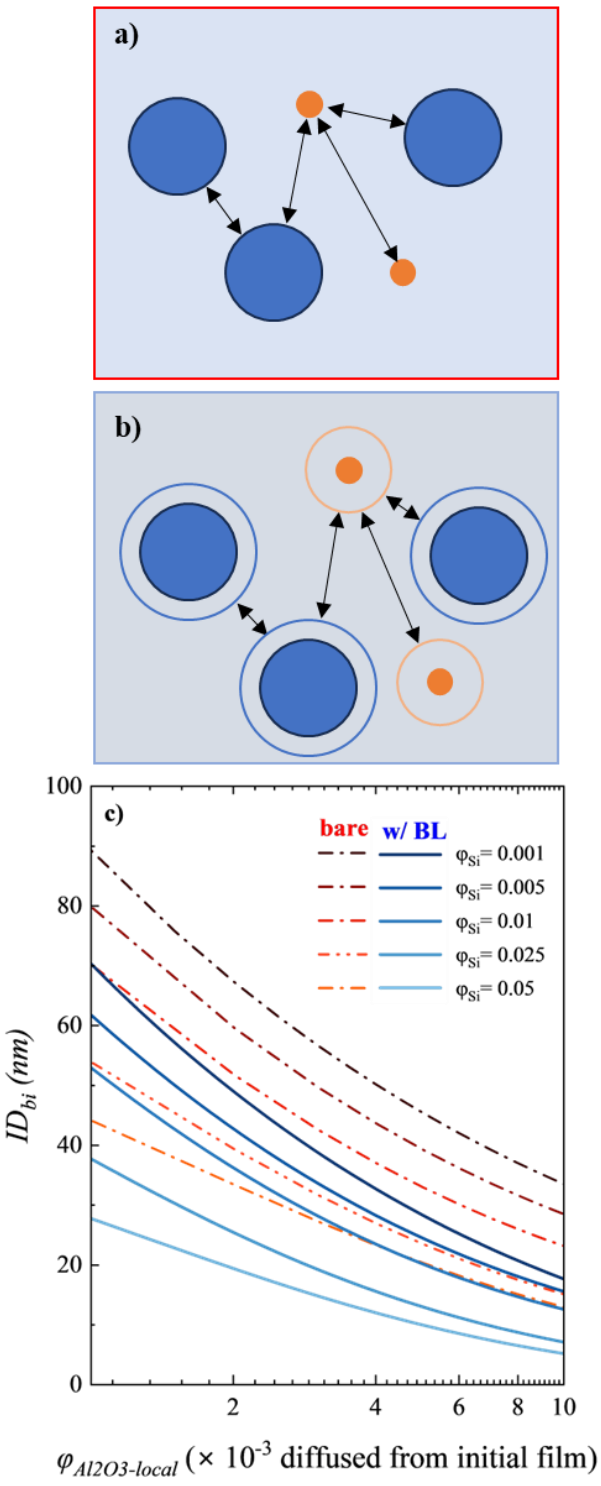

Figure 4: Schematic of ID_{bi} for a bimodal mixture of nanoparticles for bare nanoparticles **(a)** and for nanoparticles with bound polymer **(b). c)** ID_{bi} as a function of $\varphi_{Al2O3,local}$. Curves correspond to fixed values of φ_{SiO2} (0.001 to 0.050). Red dashed and blue solid lines correspond to bare NPs (r_L and r_S) and NPs with bound polymer layers ($r_{L,eff}$ and $r_{S,eff}$).

The Schweizer model[41,42] best describes the diffusion of isolated particles in polymer melts, and is proven to be an accurate model for isolated Al_2O_3 NP diffusion.[45] **Figure 5** rearranges Eqn 2 to isolate $D_{vehicleII}$ ($D_{NP} - D_{core\text{-}shell}$), which should be constant at a single M_w. We fit our data to an inverse power law scaling: $(D_{NP} - D_{core\text{-}shell} \sim (ID_{bi}/2R_{eff\text{-}Al2O3})^{-1}$ (statistically significant, $p = 0.027 < 0.05$). This deviation from a slope of 0 indicates D_{theory} alone is not an appropriate model for crowded PNCs, and the deviation becomes more significant as the length scale of confinement approaches the NP effective size.

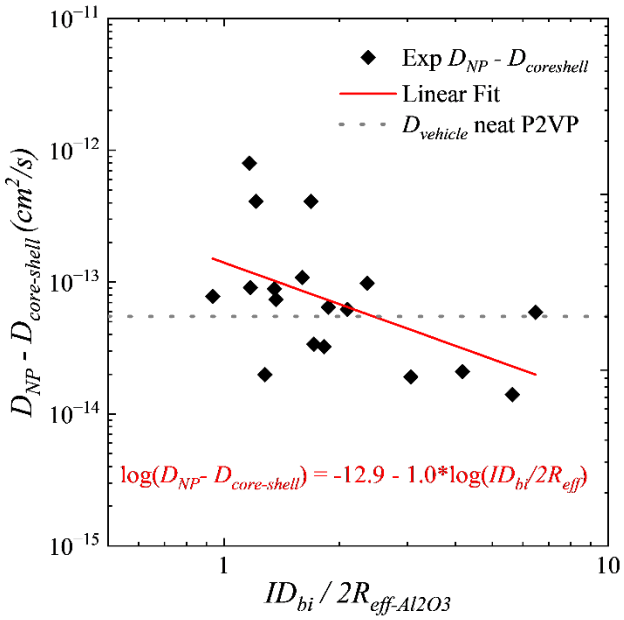

Figure 5: $D_{NP} - D_{core\text{-}shell}$ as a function of $ID_{bi}/2R_{eff\text{-}Al2O3}$ with linear regression (red) displaying an inverse power law. Dotted line is $D_{vehicle\text{-}II}$ (τ_{des} = 50 s) for neat for comparison.

As the PNC becomes more crowded, the small NPs diffuse faster than in the neat polymer. Given that the long-lived bound layer in SiO_2 PNCs are known to prevent aggregation over long-lifetimes,[24,51–53] this is somewhat counter intuitive, so we consider two contributions to NP diffusion to interpret this finding. Firstly, polymer dynamics are known to slowdown in crowded

PNC systems, but their effect on the bound layer τ_{des} is difficult to determine. Polymer diffusion coefficients (D_{poly}) are significantly depressed in PNCs at $ID < 2R_g$, and remain somewhat depressed even at $ID \sim 20R_g$.[9,18,54] Conversely, under strong geometric confinement, MD results have displayed fast polymer diffusion at intermediate levels of confinement.[55] On a segmental scale, SiO_2 P2VP PNCs displayed interfacial α-relaxation times ~ 100 times slower in loaded systems ($< \varphi = 0.15$),[56] and a greater slowdown in systems with higher interfacial area of equivalent loading.[12] The effect of chain dynamics on desorption is implied by temperature effects on bound layer exchange timescales.[57] These changes in polymer dynamics likely impact τ_{des} or change the vehicular regime (τ_{des} scaling) by changing τ_{Rouse} and τ_{Rep}, leading to faster NP diffusion. In our experiments, strongly bound P2VP on SiO_2 may decrease the free polymer available for exchange and thus alter the vehicular diffusion mechanisms and hasten NP diffusion.

Secondly, particle-induced chain disentanglement has been demonstrated experimentally, with ~ 25% dilation in d_t in highly-loaded small-NP systems (φ = 0.20), with a commensurate decrease in the bulk viscosity.[10,16] Notably, Tuteja et al. found that particle interactions at low loadings increase matrix viscosity, until reaching strong confinement conditions.[15] In attractive octaamino-phenyl polyhedral oligomeric silsesquioxan (OAPS)/P2VP (R_{OAPS} = 1.8 nm) systems, disentanglement was observed at high loading ($\varphi \sim 27\%$), but was not observed in similarly loaded SiO_2 NP ($R_{NP} \sim$ 12 nm) systems, confirming small NP size is an essential factor in chain disentanglement.[14] In our system, ID_{bi} normalized by the polymer $2R_g$ is ~ 1.7 - 10, which is not considered strong confinement ($ID/2R_g < 1$). Furthermore, our SiO_2/P2VP PNCs (R_{NP} = 26.2 nm >> R_g, φ_{SiO2} = 0.001-0.05) are unlikely to reduce the viscosity due to tube dilation and thus unlikely to be the sole cause of fast Al_2O_3 NP diffusion. Regardless, given $D_{vehicleII}$ and $D_{vehicleIII}$ scale ~ d_T, tube dilation could play a role in faster NP diffusion in crowded NP systems.

In summary, we observed faster than expected D_{NP} for small NPs diffusing into PNCs with increasing crowding. To contextualize our results, we developed a geometric model for the bimodal interparticle distance, ID_{bi}, to quantify spatial confinement. Increased crowding resulted in positive deviations of D_{NP} relative to our previously measured D_{NP} into neat polymer. We attributed this increase to greater vehicular diffusion due to (1) changes in local chain dynamics or (2) chain disentanglement induced by the NPs. Overall, these ToF SIMS experiments demonstrate a method to measure NP diffusion in complex PNCs by distinguishing NPs of different sizes in a crowded system. Future work could explore the effects of polymer molecular weight, interaction strength, and particle shape on D_{NP} in crowded and complex PNC systems.

Experimental Methods

Poly(2-vinyl pyridine) (P2VP) (158 kDa, PDI = 1.06, R_g = 10.9 nm) was obtained from Scientific Polymer Products Inc. and used as received. Silica (SiO_2) nanoparticles (R_{NP}-SiO_2 = 26.2 nm, PDI = 1.19) from Nissan-STL were transferred from methyl-ethyl ketone to methanol. Aluminum oxide (Al_2O_3) nanoparticles (R_{NP}-Al_2O_3 = 6.5 nm, PDI = 1.14) from Sigma Aldrich were prepared in a 50 g/L MeOH solution with P2VP to prevent aggregation. Trilayer samples comprised an Al_2O_3-P2VP layer (φ_{Al2O3} = 0.01, 200 ± 60 nm) sandwiched between two ~4 μm SiO_2-P2VP layers (φ_{SiO2} = 0.001, 0.005, 0.010, 0.025, 0.050). The assembled trilayer samples were annealed at 180 °C under vacuum (< 50 Pa) for 1-6 hours. ToF-SIMS experiments were conducted using a Tescan S8252X FIB-SEM equipped with a Xe^+ beam. We collected and analyzed 400 frames at 30 keV and 100 pA with 1024 × 1024 pixel resolution on positive ion mode to extract the Al_2O_3 nanoparticle diffusion coefficient. Details are provided in previous work.[30]

Acknowledgments

We acknowledge funding from NSF CBET 2034122 and NSF-NRT 2152205. We thank Dr. Jamie Ford at the Singh Center for Nanotechnology at the University of Pennsylvania for his expertise regarding ToF-SIMS, supported by NSF-MRSEC-DMR-2309043.

Supporting Information

References

(1) Bronstein, N. D.; Li, L.; Xu, L.; Yao, Y.; Ferry, V. E.; Alivisatos, A. P.; Nuzzo, R. G. Luminescent Solar Concentration with Semiconductor Nanorods and Transfer-Printed Micro-Silicon Solar Cells. *ACS Nano* **2014**, *8*, 44–53.

(2) Kwon, N. K.; Park, C. S.; Lee, C. H.; Kim, Y. S.; Zukoski, C. F.; Kim, S. Y. Tunable Nanoparticle Stability in Concentrated Polymer Solutions On the Basis of the Temperature Dependent Solvent Quality. *Macromolecules* **2016**, *20*, 25.

(3) Kumar, S. K.; Benicewicz, B. C.; Vaia, R. A.; Winey, K. I. 50th Anniversary Perspective: Are Polymer Nanocomposites Practical for Applications? *Macromolecules* **2017**, *50*, 714–731.

(4) Ge, T. Scaling Perspective on Dynamics of Nanoparticles in Polymers: Length- and Time-Scale Dependent Nanoparticle-Polymer Coupling. *Macromolecules* **2023**, *56*, 3809–3837.

(5) Bailey, E. J.; Winey, K. I. Dynamics of Polymer Segments, Polymer Chains, and Nanoparticles in Polymer Nanocomposite Melts: A Review. *Progress in Polymer Science* **2020**, *105*, 101242.

(6) Mun, E. A.; Hannell, C.; Rogers, S. E.; Hole, P.; Williams, A. C.; Khutoryanskiy, V. V. On the Role of Specific Interactions in the Diffusion of Nanoparticles in Aqueous Polymer Solutions. *Langmuir* **2014**, *30*, 308–317.

(7) Al-Obaidi, H.; Florence, A. T. Nanoparticle Delivery and Particle Diffusion in Confined and Complex Environments. *Journal of Drug Delivery Science and Technology* **2015**, *30*, 266–277.

(8) Lin, C.-C.; Parrish, E.; Composto, R. J. Macromolecule and Particle Dynamics in Confined Media. *Macromolecules* **2016**, *49*, 5755–5772.

(9) Lin, C. C.; Parrish, E.; Composto, R. J. Macromolecule and Particle Dynamics in Confined Media. *Macromolecules* **2016**, *49*, 5755–5772.

(10) Senses, E.; Ansar, S. M.; Kitchens, C. L.; Mao, Y.; Narayanan, S.; Natarajan, B.; Faraone, A. Small Particle Driven Chain Disentanglements in Polymer Nanocomposites. *Physical review letters* **2017**, *118*.

(11) Jo, K. Il; Oh, Y.; Kim, T. H.; Bang, J.; Yuan, G.; Satija, S. K.; Sung, B. J.; Koo, J. Position-Dependent Diffusion Dynamics of Entangled Polymer Melts Nanoconfined by Parallel Immiscible Polymer Films. *ACS Macro Letters* **2020**, *9*, 1483–1488.

(12) Gong, S.; Chen, Q.; Moll, J. F.; Kumar, S. K.; Colby, R. H. Segmental Dynamics of Polymer Melts with Spherical Nanoparticles. *ACS Macro Letters* **2014**, *3*, 773–777.

(13) Thakur, V. K.; Kessler, M. R. Self-Healing Polymer Nanocomposite Materials: A Review. *Polymer* **2015**, *69*, 369–383.

(14) Cheng, S.; Xie, S.-J.; Carrillo, J.-M. Y.; Carroll, B.; Martin, H.; Cao, P.-F.; Dadmun, M. D.; Sumpter, B. G.; Novikov, V. N.; Schweizer, K. S.; Sokolov, A. P. Big Effect of Small Nanoparticles: A Shift in Paradigm for Polymer Nanocomposites. *ACS Nano* **2017**, *11*, 752–759.

(15) Tuteja, A.; Mackay, M. E.; Hawker, C. J.; Van Horn, B. Effect of Ideal, Organic Nanoparticles on the Flow Properties of Linear Polymers: Non-Einstein-like Behavior. *Macromolecules* **2005**, *38*, 8000–8011.

(16) Schneider, G. J.; Nusser, K.; Willner, L.; Falus, P.; Richter, D. Dynamics of Entangled Chains in Polymer Nanocomposites. *Macromolecules* **2011**, *44*, 5857–5860.

(17) Gam, S.; Meth, J. S.; Zane, S. G.; Chi, C.; Wood, B. A.; Seitz, M. E.; Winey, K. I.; Clarke, N.; Composto, R. J. Macromolecular Diffusion in a Crowded Polymer Nanocomposite. *Macromolecules* **2011**, *44*, 3494–3501.

(18) Lin, C.-C.; Gam, S.; Meth, J. S.; Clarke, N.; Winey, K. I.; Composto, R. J. Do Attractive Polymer−Nanoparticle Interactions Retard Polymer Diffusion in Nanocomposites? **2013**, *46*, 42.

(19) Meth, J. S.; Gam, S.; Choi, J.; Lin, C. C.; Composto, R. J.; Winey, K. I. Excluded Volume Model for the Reduction of Polymer Diffusion into Nanocomposites. *Journal of Physical Chemistry B* **2013**, *117*, 15675–15683.

(20) Gam, S.; Meth, J. S.; Zane, S. G.; Chi, C.; Wood, B. A.; Winey, K. I.; Clarke, N.; Composto, R. J. Polymer Diffusion in a Polymer Nanocomposite: Effect of Nanoparticle Size and Polydispersity. *Soft Matter* **2012**, *8*, 6512.

(21) Xue, C.; Zheng, X.; Chen, K.; Tian, Y.; Hu, G. Probing Non-Gaussianity in Confined Diffusion of Nanoparticles. *Journal of Physical Chemistry Letters* **2016**, *7*, 514–519.

(22) Babayekhorasani, F.; Dunstan, D. E.; Krishnamoorti, R.; Conrad, J. C. Nanoparticle Diffusion in Crowded and Confined Media. *Soft Matter* **2016**, *12*, 8407–8416.

(23) Parrish, E.; Caporizzo, M. A.; Composto, R. J. Network Confinement and Heterogeneity Slows Nanoparticle Diffusion in Polymer Gels. *J. Chem. Phys.* **2017**, *146*, 203318.

(24) Holt, A. P.; Griffin, P. J.; Bocharova, V.; Agapov, A. L.; Imel, A. E.; Dadmun, M. D.; Sangoro, J. R.; Sokolov, A. P. Dynamics at the Polymer/Nanoparticle Interface in Poly(2-Vinylpyridine)/ Silica Nanocomposites. *Macromolecules* **2014**, *47*, 1837–1843.

(25) Bailey, E. J.; Griffin, P. J.; Composto, R. J.; Winey, K. I. Multiscale Dynamics of Small, Attractive Nanoparticles and Entangled Polymers in Polymer Nanocomposites. *Macromolecules* **2019**, *52*, 2181–2188.

(26) Wang, K.; Composto, R. J.; Winey, K. I. ToF-SIMS Depth Profiling to Measure Nanoparticle and Polymer Diffusion in Polymer Melts. *Macromolecules* **2023**, *56*, 2277–2285.

(27) Ge, T. Scaling Perspective on Dynamics of Nanoparticles in Polymers: Length- and Time-Scale Dependent Nanoparticle-Polymer Coupling. *Macromolecules* **2023**, *56*, 3809–3837.

(28) Shen, J.; Li, X.; Shen, X.; Liu, J. Insight into the Dispersion Mechanism of Polymer-Grafted Nanorods in Polymer Nanocomposites: A Molecular Dynamics Simulation Study. **2017**.

(29) Bailey, E. J.; Griffin, P. J.; Composto, R. J.; Winey, K. I. Characterizing the Areal Density and Desorption Kinetics of Physically Adsorbed Polymer in Polymer Nanocomposite Melts. *Macromolecules* **2020**, *53*, 2744–2753.

(30) Wang, K.; Composto, R. J.; Winey, K. I. ToF-SIMS Depth Profiling to Measure Nanoparticle and Polymer Diffusion in Polymer Melts. *Macromolecules* **2023**, *56*, 2277–2285.

(31) Lin, C.-C.; Gam, S.; Meth, J. S.; Clarke, N.; Winey, K. I.; Composto, R. J. Do Attractive Polymer−Nanoparticle Interactions Retard Polymer Diffusion in Nanocomposites? **2013**, *46*, 42.

(32) Lin, C.-C.; Ohno, K.; Clarke, N.; Winey, K. I.; Composto, R. J. Macromolecular Diffusion through a Polymer Matrix with Polymer-Grafted Chained Nanoparticles. *Macromolecules* **2014**, *47*, 5357–5364.

(33) Mills, P. J.; Green, P. F.; Palmstrom, C. J.; Mayer, J. W.; Kramer, E. J. Analysis of Diffusion in Polymers by Forward Recoil Spectrometry. *Appl Phys Lett* **1998**, *45*, 957.

(34) Composto, R. J.; Mayer, J. W.; Kramer, E. J.; White, D. M. Fast Mutual Diffusion in Polymer Blends. *Phys. Rev. Lett.* **1986**, *57*, 1312–1315.

(35) Baker, P. A.; Gieskes, J. M.; Elderfield, H.; Garrison, R. E.; Hein, J. R.; Anderson, T. F.; Katz, A.; Sass, E.; Starinsky, A.; Holland, H. D.; Kroopnick, P.; Weiss, R. F.; Craig, H. Mutual Diffusion in a Miscible Polymer Blend. *Douglas, R. G. & Savin, S.M. !nit. Rep. DSDP* **1976**, *81*, 1183–1191.

(36) Gam, S.; Meth, J. S.; Zane, S. G.; Chi, C.; Wood, B. A.; Seitz, M. E.; Winey, K. I.; Clarke, N.; Composto, R. J. Macromolecular Diffusion in a Crowded Polymer Nanocomposite. *Macromolecules* **2011**, *44*, 3494–3501.

(37) Composto, R. J.; Kramer, E. J.; White, D. M. Fast Macromolecules Control Mutual Diffusion in Polymer Blends. *Nature* **1987**, *328*, 234–236.

(38) Choi, J.; Clarke, N.; Winey, K. I.; Composto, R. J. Fast Polymer Diffusion through Nanocomposites with Anisotropic Particles. *ACS Macro Lett.* **2014**, *3*, 886–891.

(39) Cole, D. H.; Shull, K. R.; Rehn, L. E.; Baldo, P. M. RBS Analysis of the Diffusion of Nano-Size Spheres in a Polymer Matrix. *Nucl Instrum Methods Phys Res B* **1998**, *136–138*, 283–289.

(40) Griffin, P. J.; Bocharova, V.; Middleton, L. R.; Composto, R. J.; Clarke, N.; Schweizer, K. S.; Winey, K. I. Influence of the Bound Polymer Layer on Nanoparticle Diffusion in Polymer Melts. *ACS Macro Lett* **2016**, *5*, 1141–1145.

(41) Carroll, B.; Bocharova, V.; Carrillo, J.-M. Y.; Kisliuk, A.; Cheng, S.; Yamamoto, U.; Schweizer, K. S.; Sumpter, B. G.; Sokolov, A. P. Diffusion of Sticky Nanoparticles in a Polymer Melt: Crossover from Suppressed to Enhanced Transport. *Macromolecules* **2018**, *51*, 2268–2275.

(42) Yamamoto, U.; Carrillo, J.-M. Y.; Bocharova, V.; Sokolov, A. P.; Sumpter, B. G.; Schweizer, K. S. Theory and Simulation of Attractive Nanoparticle Transport in Polymer Melts. *Macromolecules* **2018**, *51*, 2258–2267.

(43) Griffin, P. J.; Bocharova, V.; Middleton, L. R.; Composto, R. J.; Clarke, N.; Schweizer, K. S.; Winey, K. I. Influence of the Bound Polymer Layer on Nanoparticle Diffusion in Polymer Melts. *ACS Macro Letters* **2016**, *5*, 1141–1145.

(44) Park, J.; Bailey, E. J.; Composto, R. J.; Winey, K. I. Single-Particle Tracking of Nonsticky and Sticky Nanoparticles in Polymer Melts. *Macromolecules* **2020**, *53*, 3933–3939.

(45) Wang, K.; Winey, K. I. Vehicular and Core-Shell Nanoparticle Diffusion in Entangled Polymer Melts. *Macromolecules* **2024**, *57*, 6789–6795.

(46) Bailey, E. J.; Griffin, P. J.; Composto, R. J.; Winey, K. I. Multiscale Dynamics of Small, Attractive Nanoparticles and Entangled Polymers in Polymer Nanocomposites. *Macromolecules* **2019**, *52*, 2181–2188.

(47) Skóra, T.; Vaghefikia, F.; Fitter, J.; Kondrat, S. Macromolecular Crowding: How Shape and Interactions Affect Diffusion. *J. Phys. Chem* **2020**, *124*, 7537–7543.

(48) Hao, T.; Riman, R. E. Calculation of Interparticle Spacing in Colloidal Systems. *Journal of Colloid and Interface Science* **2006**, *297*, 374–377.

(49) Jouault, N.; Moll, J. F.; Meng, D.; Windsor, K.; Ramcharan, S.; Kearney, C.; Kumar, S. K. Bound Polymer Layer in Nanocomposites. *ACS Macro Lett* **2013**, No. 2, 371–374.

(50) Starr, F. W.; Douglas, J. F.; Meng, D.; Kumar, S. K. Bound Layers "Cloak" Nanoparticles in Strongly Interacting Polymer Nanocomposites. *ACS Nano* **2016**, *10*, 10960–10965.

(51) Jimenez, A. M.; Zhao, D.; Misquitta, K.; Jestin, J.; Kumar, S. K. Exchange Lifetimes of the Bound Polymer Layer on Silica Nanoparticles. *ACS Macro Lett* **2019**, *8*, 166–171.

(52) Jouault, N.; Zhao, D.; Kumar, S. K. Role of Casting Solvent on Nanoparticle Dispersion in Polymer Nanocomposites. **2014**.

(53) Wei, T.; Torkelson, J. M. Molecular Weight Dependence of the Glass Transition Temperature (Tg)-Confinement Effect in Well-Dispersed Poly(2-Vinyl Pyridine)-Silica Nanocomposites: Comparison of Interfacial Layer Tgand Matrix Tg. *Macromolecules* **2020**, *53*, 8725–8736.

(54) Bailey, E. J.; Riggleman, R. A.; Winey, K. I. Polymer Conformations and Diffusion through a Monolayer of Confining Nanoparticles. *Macromolecules* **2020**, *53*, 8171–8180.

(55) Pressly, J. F.; Riggleman, R. A.; Winey, K. I. Polymer Diffusion Is Fastest at Intermediate Levels of Cylindrical Confinement. *Macromolecules* **2018**, *51*, 9789–9797.

(56) Holt, A. P.; Griffin, P. J.; Bocharova, V.; Agapov, A. L.; Imel, A. E.; Dadmun, M. D.; Sangoro, J. R.; Sokolov, A. P. Dynamics at the Polymer/Nanoparticle Interface in Poly(2-Vinylpyridine)/ Silica Nanocomposites. *Macromolecules* **2014**, *47*, 1837–1843.

(57) Jimenez, A. M.; Zhao, D.; Misquitta, K.; Jestin, J.; Kumar, S. K. Exchange Lifetimes of the Bound Polymer Layer on Silica Nanoparticles. *ACS Macro Letters* **2019**, *8*, 166–171.